Structural elucidation and environmental distributions of butanetriol and pentanetriol dialkyl glycerol tetraethers (BDGTs and PDGTs)

Sarah Coffinet[1]; Travis B. Meador[1,*]; Lukas Mühlena[1]; Kevin W. Becker[1,**]; Jan Schröder[1]; Qing-Zeng Zhu[1]; Julius S. Lipp[1]; Verena B. Heuer[1]; Matthew P. Crump[2]; Kai-Uwe Hinrichs[1]

[1]MARUM – Center for Marine Environmental Sciences, University of Bremen, Germany
[2]School of Chemistry, University of Bristol, United Kingdom

Correspondence to: Sarah Coffinet (scoffinet@marum.de)

Present addresses:

* Biology Centre CAS, SoWa-RI, České Budějovice, Czechia

** GEOMAR Helmholtz Centre for Ocean Research, Kiel, Germany

Abstract. Butanetriol and pentanetriol dialkyl glycerol tetraethers (BDGTs and PDGTs) are membrane lipids recently discovered in sedimentary environments and in the methanogenic archaeon *Methanomassiliicoccus luminyensis*. They possess an unusual structure, which challenges fundamental assumptions in lipid biochemistry. Indeed, they bear a butanetriol or a pentanetriol backbone instead of a glycerol at one end of their core structure. In this study, we unambiguously located the additional methyl group of the BDGT compound on the C3 carbon of the lipid backbone via high-field NMR experiments. We further systematically explored the abundance, distribution and isotopic composition of BDGTs and PDGTs as both intact polar and core lipid forms in marine sediments collected in contrasting environments of the Mediterranean Sea and Black Sea. High proportions of intact polar BDGTs and PDGTs in the deeper methane-laden sedimentary layers and relatively ^{13}C-depleted BDGTs, especially in the Rhone delta and in the Black Sea, are in agreement with a probable methanogenic source for these lipids. However, contributions from heterotrophic archaea to BDGTs (and PDGTs) cannot be excluded, particularly in the eastern Mediterranean Sea, and contrasting BDGT and PDGT headgroup distribution patterns were observed between the different studied sites. This points to additional, non-methanogenic, archaeal sources for these lipids.

1 Introduction

Unique membrane lipids were a key argument to postulate the existence of Archaea as a third and independent domain of life, as distantly related to Bacteria as to Eukarya, when Woese et al. (1990) proposed their revised tree of life. Membrane lipids form an envelope that separates cells from their environment and protects their interior components. Specific chemical properties define the fluidity and permeability of the membrane barrier, regulating what can enter the internal cell compartment. On the one hand, membrane lipids from members of all domains of life share some common characteristics, such as their amphiphilic nature. That is, they all possess apolar alkyl chains and polar headgroups held together by a glycerol moiety (Lombard et al., 2012). On the other hand, membrane lipids of Archaea fundamentally differ from those of Bacteria and Eukarya in that they contain (bi)phytanyl chains constituted from the condensation of several isoprenoid units and ether linkages to the *sn*2 and *sn*3 carbons of a glycerol backbone (De Rosa and Gambacorta, 1988; Koga and Morii, 2005). On the contrary, Bacteria and Eukarya generally produce fatty acyl chains linked to the sn1 and sn2 carbons of the glycerol backbone (Kates, 1977). Intensive exploratory analyses of lipid extracts from pure cultures and environmental samples over the last decades (e.g. Elling et al., 2017; Koga et al., 1993; Koga and Morii, 2005; Liu et al., 2012; Meador et al., 2014; Paściak et al., 2003; Schouten et al., 2000, 2013; Sturt et al., 2004; Weijers et al., 2006), revealed a large diversity of membrane lipids and a more complex picture than first considered by Woese et al. (1990). Several non-isoprenoid ether glycerol lipids were identified as of bacterial origin, such as the branched glycerol dialkyl glycerol tetraethers (brGDGTs, Weijers et al., 2006) or the alkyl

glycerol ether lipids (AGEs; e.g. Hinrichs et al., 2000; Pancost et al., 2001; Rütters et al., 2001). To date, AGEs have been observed in a wide range of pure cultures, covering different bacterial phyla with contrasting physiologies (Vinçon-Laugier et al., 2016). In addition, lipids containing both a (bi)phytanyl and a non-isoprenoidal alkyl chain were previously observed in natural environments (Liu et al., 2012; Schouten et al., 2000). Nevertheless, all the above-mentioned membrane lipids possess glycerol backbones, which appear to be a common feature shared by members of all domains of life.

The recent identification of butanetriol and pentanetriol dialkyl glycerol tetraethers (BDGTs and PDGTs, Knappy et al., 2014; Zhu et al., 2014), in which one glycerol is substituted by a butanetriol or pentanetriol, challenges this assumption. Tandem mass spectrometry complemented with gas chromatography (GC) detection of butanetriol after hydrolysis (Zhu et al., 2014) demonstrated the presence of a 1,2,3 butanetriol backbone in BDGTs but did not specify its configuration within the lipid molecule, notably its linkages with the biphytanyl side chains. Subsequently, BDGTs and PDGTs were observed in diverse samples, both as intact polar lipids (IPLs, lipids with polar headgroups) and core lipids (CLs, lipids without polar headgroups), from recent organic-rich estuarine sediments (Meador et al., 2015) to old Jurassic marine shales (Knappy et al., 2014) and deep subsurface sediments (Becker et al., 2016; Zhu et al., 2014). Furthermore, Becker et al. (2016) identified BDGTs as prominent membrane lipids in *Methanomassiliicoccus luminyensis*, currently the only cultured representative of the seventh order of methanogens; lower quantities of PDGTs were also observed in this archaeon. BDGTs accounted for up to 82% of the detected core lipids, while being absent from 25 different pure cultures spanning the main archaeal phyla and encompassing several representatives of the different orders of methanogens, thus leading to the conclusion that the capability to synthesize BDGTs and PDGTs among the methanogens could potentially be restricted to the order Methanomassiliicoccales (Becker et al., 2016). However, this exclusive chemotaxonomic relationship contrasts with the wide diversity of geochemical settings where BDGTs and PDGTs have been detected and cultured representatives for several archaea phyla remain unavailable for screening. For example, Meador et al. (2015) had suggested members of the Miscellaneous Crenarchaeotal Group, now termed Bathyarchaeota, as a source of BDGTs in the estuarine White Oak River Basin due to the similarly high relative abundances and correlation of BDGTs with bathyarchaeotal 16S genes in the sediment profile.

In the present study, the exact structure of the core BDGT molecule was elucidated through high-field two-dimensional NMR analysis of BDGT purified from a pure culture of *M. luminyensis*. In addition, the relative abundance of BDGTs and PDGTs and stable carbon isotopic composition (δ^{13}C) of BDGTs were systematically investigated in a set of 48 marine sediment samples covering a wide range of environmental and geochemical conditions. Our aim was to provide new insights into the diversity and carbon metabolism of BDGT and PDGT producers and on the potential roles of these novel lipids in the cell membrane.

2 Material and Methods

2.1 Sample collection

Marine sediment samples were collected with a combination of multi-corer and gravity coring at eight different sites (Fig. 1) in the Mediterranean and Black Seas during two expeditions: RV *Meteor* Cruise M84/1 (Zabel et al., 2011) and RV *Poseidon* Cruise POS450 (Heuer et al., 2014). Description of the environmental characteristics, geochemical and sedimentary conditions of the eight visited sites can be found in Schmidt et al. (2017). From these locations, 48 samples spanning different environments and geochemical conditions were selected for detailed organic geochemical investigation (Suppl. Table 1).

2.2 Marine sediment lipid extraction and quantification

Lipid extraction of sediment samples was performed according to a modified Bligh & Dyer method (Sturt et al., 2004). All frozen sediment samples were homogenized at −196 °C using a CryoMill (Retsch), which was operated as follows: two cycles of pre-cooling for 2 min each, with a speed of the impactor of 5 impacts s⁻¹ and homogenizing and fragmenting for 2 min with

25 impacts s^{-1}. Samples (ca. 50-60 g wet weight) were then lyophilized and ultrasonically extracted four times with a mixture

80   of DCM/MeOH/buffer (1:2:0.8; v:v:v), with a phosphate buffer at pH 7.4 for the first two steps and a trichloroacetic acid buffer at pH 2.0 for the remaining two steps. The sample was extracted in two final steps with DCM/MeOH (5:1). Each extraction step was followed by centrifuging the samples for 10 min and the resulting supernatants were combined in a separatory funnel. An equal amount of DCM and Milli-Q water was added to the supernatants and the separatory funnel was thoroughly mixed. After phase separation the aqueous phase was washed three times with DCM and the water phase was

85   discarded. The organic phase was washed three times with Milli-Q water, collected and evaporated to dryness under a stream of N$_2$. The total lipid extracts (TLE) obtained were stored at -20 °C until further analysis.

Detection and quantification of intact polar lipids (IPLs) were carried out on a maXis plus ultra-high resolution quadrupole-time-of-flight mass spectrometer (Q-ToF-MS; Bruker), coupled to an Ultimate 3000RS ultra high pressure liquid chromatography instrument (UHPLC; Dionex). IPLs were chromatographically separated by an ACE3 C18 column (150 x 2.1

90   mm; particle size 3 μm; ACE) as described by Zhu et al. (2013) and detected in positive ionization mode scanning a mass range of 150 – 2000 Da. Lipids were identified by retention time, exact mass (± 0.001 Da), and characteristic fragmentation patterns obtained by data-dependent MS² scans. IPLs were quantified by comparison of the intensity of parent ions with that of a C$_{46}$-glycerol trialkyl glycerol tetraether (GTGT; Huguet et al., 2006) added as an internal standard. IPL concentrations were corrected for their response factors determined from purified and commercially available standards following the

95   procedure described by Becker et al. (2016).

2.3 Stable carbon isotope analysis

Six of the 48 marine sediment TLE from the Rhone delta, the eastern Mediterranean Sea and the Black Sea (Samples # 5, 8, 20, 22, 34, 38 of the dataset; detailed information available in Suppl. Table 1) were selected to investigate the natural stable isotopic composition of the BDGT-derived biphytanes. Only IPL-BDGTs were analyzed as they are more likely to derive from

100   living organisms. Before isotopic analysis via gas chromatography coupled to isotope ratio mass spectrometry (GC-IRMS), IPL-BDGTs were purified with two steps of preparative HPLC and then cleaved into biphytanes (bp), as detailed below.

2.3.1 Preparative HPLC

TLE samples were first separated into IPL and CL fractions by preparative HPLC (Agilent 1200 series) with a modified version of the protocol reported by Meador et al. (2015). TLE separation was performed on an LiChrospher Diol column (250 x 10

105   mm; 5 μm, Grace) with *n*-hexane/isopropanol (90:10; v/v) as eluent A and 100% isopropanol as eluent B. Chromatographic conditions were as follows: a gradient from 100% A at 3 ml min^{-1} to 24% B in 15 min and then to 100% B in 5 min at a flow rate of 2 ml min^{-1}. 100% B at 2 ml min^{-1} was maintained for 10 min before switching back to the initial conditions for 15 min. During the run, the eluent flow was split (split ratio 150:1; Agilent active splitter G1968D) between the fraction collector and an online mass spectrometer (Agilent 6130 single quadrupole) allowing continuous monitoring of retention time stability.

110   Fraction 1 (F1), containing the CLs, was collected from 0 to 7 min and fraction 2 (F2), containing the IPLs, from 11 to 30 min. The collected fractions were subsequently dried under a stream of N$_2$. IPLs were then converted into CLs by acid hydrolysis with 1 M HCl in MeOH for 3 h at 70 °C (Pitcher et al., 2009; Elling et al., 2014).

CL-BDGTs were further separated from CL-GDGTs according to Zhu et al. (2014). The hydrolyzed IPL fraction was injected into an Agilent 1200 normal phase HPLC-system equipped with a PerfectSil CN-3 column (250 x 10 mm, 5 μm, MZ

115   Analysentechnik). Separation was achieved at a flow rate of 2.5 ml min^{-1} with an elution gradient from 100% A (99:1 *n*-hexane:isopropanol) held for 5 min, ramping to 10% B (90:10 *n*-hexane:isopropanol) at 12 min and then to 100% B at 30 min finally holding 100% B for 12 more min. The solvent system was then returned to initial conditions for 10 min. Retention time stability was monitored via simultaneous MS detection as above. BDGTs and GDGTs were collected between 13 and 16 min and between 16 and 21 min, respectively.

2.3.2 Ether cleavage and compound specific stable carbon isotope analysis

Ether cleavage with BBr_3 was performed on the purified CL-BDGT and CL-GDGT fractions to convert them into biphytanes (bp) following the protocol by Kellermann et al. (2012). Briefly, aliquots of the dried fractions were amended with 200 μl of 1 M BBr_3 dissolved in DCM and incubated in sealed tubes at 60 °C for 2 h followed by reduction with 200 μl of 1 M superhydride in tetrahydrofuran. Liquid-liquid extraction with H_2O and *n*-hexane was performed three times and the aqueous phase was discarded. The apolar phase was purified on a silica column with *n*-hexane as eluent. Carbon isotopic composition of biphytanes was measured on a Trace GC Ultra coupled to a GC-IsoLink ConFlow IV interface and a Delta V Plus IRMS (Thermo) equipped with a Rxi-5ms column (30 m x 250 μm x 0.25 μm, Restek). The injection temperature was set at 300 °C; the initial oven temperature was held at 60 °C for 1 min, followed by an increase to 150 °C at 10 °C min^{-1} and then to 320 °C at 4 °C min^{-1} with a flow rate of 1.2 ml min^{-1}. Every sample was measured in duplicate and the associated error was lower or equal to 1‰.

2.4 Stable carbon isotope composition of potential carbon sources

In order to gain information on the C sources of BDGTs, the stable carbon isotope analysis of the total organic carbon (TOC), the dissolved inorganic carbon (DIC) and methane (CH_4) was determined. TOC content and stable carbon isotopic analysis ($\delta^{13}C_{TOC}$) were previously described in Schmidt et al. (2017). Stable carbon isotopic analysis of DIC ($\delta^{13}C_{DIC}$) and CH_4 ($\delta^{13}C_{CH4}$) were measured on shore within the year following each cruise. Prior to analysis, pore water aliquots of 2 ml were stored at -20 °C in vials without headspace for $\delta^{13}C_{DIC}$ analysis and ca. 3 ml of sediment were stored at 4 °C in 22 ml gas tight vials amended with 5 ml NaOH for $\delta^{13}C_{CH4}$ analysis. $\delta^{13}C_{DIC}$ was measured using a gas bench coupled to a Finnigan MAT 252 mass spectrometer. Samples were prepared as follows: 100 μl of phosphoric acid were transferred to glass tubes, which were subsequently sealed with butyl septa and plastic caps and purged five times with helium. Fluid samples (0.2–1.0 ml) were injected into the purged tubes by syringe and allowed to degas CO_2 from the acidified aqueous matrix for at least five hours. Carbon isotopic compositions of CO_2 were then analyzed in subsamples of the gas phase. The precision of the analysis was 0.1‰ (1σ). CH_4 stable carbon isotope values were determined on a Trace GC Ultra coupled to a GC combustion III interface and a Delta Plus XP IRMS (Thermo) equipped with a Carboxen 1006 Plot column (Supelco, Sigma Aldrich). Injection temperature was set at 200 °C, the oven temperature was held at 40 °C for 6 min and the flow rate at 3 ml min^{-1}.

2.5 Cultivation of *Methanomassiliicoccus luminyensis*, lipid extraction and BDGT-0 purification for NMR analysis

M. luminyensis strain was purchased at DSMZ (Leibniz Institute DSMZ – German Collection of Microorganisms and Cell Cultures) and grown in an anaerobic medium optimized by the DSMZ (protocol 1637). A total volume of 2 l of culture was grown in two 2 l Schott bottles, inoculated with 10% (v/v) of a previous culture grown under the same conditions, i.e. at 37 °C under an atmosphere containing 80% H_2 and 20% CO_2. After 16 days, cells were harvested by centrifugation (25 min; 4500 rpm) and were subsequently lyophilized.

Direct acid hydrolysis of the freeze-dried biomass pellet was performed according to Becker et al. (2016) using 1 M HCl in MeOH for 16 h at 70 °C. CLs were extracted by ultra-sonication (two times 20 min) with a 5:1 DCM:MeOH solvent mix and the extracts were collected in a separatory funnel. Lipids were partitioned into the organic phase following addition of Milli-Q H_2O. The water phase was then extracted three times with an equal amount of DCM. The organic phases were pooled in an Erlenmeyer flask before transfer into the separation funnel and further washing (three times) with an equal amount of Milli-Q H_2O. The water phase was discarded and the organic solvent was evaporated under a gentle flow of N_2. CL-BDGT-0 was purified by preparative HPLC following the same preparative HPLC protocol as described in Section 2.3.1. BDGT-0 was collected between 12.3 and 13 min. BDGT-0 was estimated to be pure at 99.4% via UHPLC-QToF-MS following the protocol by Becker et al. (2015).

2.6 NMR analysis

BDGT-0 (860 μg) was dissolved in CDCl$_3$ (170 μL) and transferred to a 3 mm NMR tube. ^{1}H, ^{13}C spectra and two-dimensional COSY, TOCSY, ^{1}H-^{13}C HSQC and ^{1}H-^{13}C HMBC were acquired at 600 MHz on a Varian VNMRS spectrometer equipped with triple resonance ^{1}H observe cryogenic probe. Spectra were processed and analyzed using VnmrJ 4.2 software provided with the spectrometer.

2.7 Statistical analysis

Principal component analysis (PCA) was performed with the R software using factominR and vegan packages. PCA requires all variables to follow a normal distribution, thus all data were reduced and centered before analysis.

3 Results

3.1 NMR analysis of BDGT-0 extracted from *M. luminyensis*

Analysis of high-resolution ^{1}H and ^{13}C one-dimensional spectra revealed a number of downfield signals (3.15-3.70 ppm) that suggested desymmetrization when compared to the expected number of signals from, for example, GDGT-0 (Supplementary Figure 1; Sinninghe Damsté et al., 2002). Analysis of two-dimensional spectra (^{1}H-^{13}C HSQC and HMBC, ^{1}H-^{1}H COSY and TOCSY, Table 1) revealed one set of ^{1}H and ^{13}C chemical shifts closely matching the assignments of the glycerol components and ether linked CH$_2$ groups of GDGT-0 (Table 1; Sinninghe Damsté et al., 2002). These included the characteristic methine signal of C2 and methylene signals of C1 and C3 (Supplementary Figure 2B) that could be connected via HMBC correlations (e.g. C1 correlated to C2 and C3) and ^{1}H connectivities. The resolved diastereotopic protons 3.68 ppm to 3.58 ppm (C1 protons), 3.51 and 3.44 ppm (C3 protons) and 3.49 (C2 proton) also confirmed these assignments. Multiplicity editing (opposite signal phases for methyl/methine and methylene signals) applied in the ^{1}H-^{13}C HSQC spectra assisted in this assignment and in distinguishing the glycerol/butanetriol moieties and their unique distribution of methyl/methine and methylene signals as detailed below. C3 could be correlated with A1 via ^{1}H-^{13}C HMBC correlations through the ether linkage (Supplementary Figure 3) and A1 and B1 were linked to A2/A3 and B2 respectively also via HMBC.

However, a number of new *O*-linked methine (C2' and C3') and methylene signals (A1', B1' and C1') were visible compared to ^{1}H-^{13}C HSQC spectra of GDGT-0 as well as an additional aliphatic methyl signal (C4', 16.62 ppm; Supplementary Figures 1-3). The strong C4' signal appeared as a doublet in the 1D ^{1}H spectrum (Supplementary Figure 1), albeit overlapped and consistent with coupling to the single C3' methine proton. C4' showed clear correlations via HMBC to both C3' and C2' (Supplementary Figure 3, annotated) and well-resolved ^{1}H correlations in the ^{1}H-^{1}H COSY/TOCSY spectra to the C1', C2' and C3' protons. The characteristic downfield ^{13}C shift of C2' also gave resolved correlations to C1' and C3'. C2' and C3' could then be correlated via HMBC through their ether linkages to resolved *O*-linked CH$_2$ signals (A1' and B1'). Similarly, A1' and B1' could be correlated to A2' and B2' respectively as both were partially resolved from A2 and B2. A3/3' and B3/3' appeared to give a single methine resonance in the ^{1}H-^{13}C HSQC spectrum but were partially resolved in the ^{1}H-^{13}C HMBC, showing A3 and A3' could be distinguished by their ^{13}C chemical shifts (29.71 and 29.54 ppm respectively) and were resolved from B3/3' (29.60 ppm). Aside from this, the remainder of the (highly overlapped) branched alkyl chain chemical shifts (from A4'/B4' onwards, Supplementary Figure 2A) were superimposable on those of GDGT-0 suggesting an identical arrangement of branched methyl groups (Table 1). Together these analyses confirmed the presence of a butanetriol group at the opposing end of the molecule (Fig. 2) and four resolvable ether linkages.

3.2 BDGT and PDGT in the Mediterranean and Black Sea sediments

3.2.1 BDGT and PDGT abundance and diversity

Geochemical parameters of the 48 analyzed samples were previously described in Schmidt et al. (2017). Notably, TOC values ranged between 0.08 and 4.37% (Suppl. Table 1). The highest TOC content was measured in the sapropel layers of the eastern Mediterranean Basin (GeoB15103) while the basin sites, i.e. eastern Mediterranean Basin (excluding the sapropel layers), Cap de Creus Canyon and Ligurian-Provençal Basin (GeoB15103, GeoB17302, GeoB17304), exhibited the lowest TOC contents. From the 48 samples, ranging in depth from surface to 635 cm and ages from modern to ~173,000 years, BDGTs and PDGTs were detected as CLs and IPLs in 45 and 37 samples, respectively. PDGTs were not detected in samples from the Black Sea (GeoB15105). Concentrations ranged from 0.04 to 9.2 µg g^{-1} C_{org} for BDGTs and from 0.04 to 3.1 µg g^{-1} C_{org} for PDGTs, which correspond, in average, to 8 and 3% of the GDGT-0 concentration in these samples, respectively (Suppl. Table 2). BDGT structures with up to 2 cycloalkyl rings were assigned based on their retention time and MS^2 spectra but BDGT-0 was generally predominant (Suppl. Table 2). IPL-BDGTs and IPL-PDGTs comprised mono- (1G) and diglycosidic (2G) lipids. The relative abundance of these IPLs within the total pool comprised of both the corresponding CLs and IPLs (on average, 74% for IPL-BDGTs and 93% for IPL-PDGTs) was much higher than the relative abundance of IPL-GDGTs (18% on average; Suppl. Table 2 and Fig. 3).

3.2.2 Principal Component Analysis (PCA) on BDGT and PDGT distribution

In order to evaluate the variability in BDGT and PDGT distribution within the dataset, a PCA was performed with the major environmental variables and indices of BDGT and PDGT relative abundances. In addition to the fractional abundance for each BDGT and PDGT pool [f(CL-BDGTs), f(1G-BDGTs), f(2G-BDGTs), f(CL-PDGTs), f(1G-PDGTs), f(2G-PDGTs)], the relative proportion of IPLs to the total lipid content [f(IPL-BDGTs), f(IPL-PDGTs)] and the relative proportion of BDGTs and PDGTs to the total GDGT-0 content [(sum-BDGTs)/(sum-GDGT-0), (sum-PDGTs)/(sum-GDGT-0)] were computed (Suppl. Table 2). This PCA separated three groups of samples that differed from their geochemical properties and their BDGT and PDGT content (Fig. 4). The first group contained all samples from the Rhone delta (sites GeoB17306, 7, 8) and is characterized by high concentrations of dissolved Fe and CH_4, shallow water depths, and relatively low values of $\delta^{13}C_{TOC}$ (Fig. 4). This sample group shows a high proportion of BDGTs and PDGTs relative to GDGT-0, and a high proportion of IPL-BDGTs and IPL-PDGTs, especially as diglycosidic lipids (2Gs; Fig. 4). The second group of samples includes all samples collected in the Black Sea (GeoB15105), with high concentrations of DIC, DOC, and HS$^-$, and a low concentration of SO_4^{2-}. The last group comprises all samples from basin sites, which are characterized by relatively lower TOC and lower terrestrial input, i.e. from the eastern Mediterranean basin (GeoB15103), the Marmara Sea (GeoB15104) and Cap de Creus and Ligurian-Provençal Basin (GeoB17302 and 17304). These samples all exhibit high water depth, less negative $\delta^{13}C_{TOC}$ values and higher concentrations in SO_4^{2-}. The Black Sea and basin site groups are characterized by higher contributions of CL- and 1G-BDGTs than the first group of river delta samples. Moreover, the Black Sea group differs from the other groups by its high proportion of CL-BDGTs and its lack of PDGTs (both CL and IPL) while the basin sites are relatively enriched in 1G-PDGTs (Fig. 4).

3.2.3 Stable carbon isotopic composition of BDGT-0

Six samples were selected for analysis of the ^{13}C isotopic composition (δ^{13}C) of the IPL-BDGT derived biphytanes. A dedicated preparative LC protocol enabled comparison of δ^{13}C of bp-0 from IPL-BDGT-0 ($\delta^{13}C_{BDGTs}$) with that derived of bp-0 from IPL-GDGT-0 ($\delta^{13}C_{GDGTs}$). At all sites, $\delta^{13}C_{BDGTs}$ was more depleted than $\delta^{13}C_{GDGTs}$. Both Black Sea (GeoB15105) and Rhone delta (GeoB17306) sites showed very negative $\delta^{13}C_{BDGTs}$ values of -56±1‰ and -41±1‰ while the $\delta^{13}C_{BDGTs}$ were around -28±0.1‰ in the sapropel layers of the eastern Mediterranean basin (Fig. 5). Bp-0 from both BDGTs and GDGTs were more

enriched in ^{13}C than CH_4 in each sample. On the contrary, they were more depleted in ^{13}C relative to DIC. In addition, $\delta^{13}C_{GDGTs}$ values were generally similar to $\delta^{13}C_{TOC}$, while $\delta^{13}C_{BDGTs}$ values were more negative (Fig. 5).

4 Discussion

4.1 Potential source organisms of BDGTs and PDGTs

240   $\delta^{13}C$ analysis of membrane lipids in environmental samples provides insight into the carbon metabolism that promoted their biosynthesis and can thus help to assign their source organisms (Hayes, 2001; Pearson, 2010). In this study, six marine sediment samples exhibiting relatively high concentrations of BDGTs and representing contrasting geochemical settings were selected for $\delta^{13}C$ analysis of lipid biomarker and carbon substrate pools to investigate the potential drivers of BDGT distributions in the environment. PDGT concentrations were too low to be analyzed for their carbon isotopic composition. BDGT-derived

245   biphytanes ($\delta^{13}C_{BDGTs}$) exhibited systematically more negative $\delta^{13}C$ values than GDGT-derived biphytanes ($\delta^{13}C_{GDGTs}$) at all sites, pointing to a distinct origin of BDGTs (Fig. 5). Moreover, the range of $\delta^{13}C_{BDGTs}$ (between -56 and -28‰) is suggestive of a predominant benthic rather than planktonic source for these compounds (Hoefs et al., 1997; Pearson et al., 2001). Accordingly, IPL-BDGTs and IPL-PDGTs, supposedly representative of extant organisms, constituted more than 50% of the whole BDGT and PDGT pool in more than 90% of the sediment samples where they were detected (Fig. 3 and Suppl. Table

250   2), further supporting a benthic origin of BDGTs and PDGTs.

In the Black Sea and Rhone delta (GeoB15105 and GeoB17306), BDGT-derived biphytanes had similarly low $\delta^{13}C$ values (i.e., < -40‰), suggesting that BDGTs were derived from functionally related archaeal phyla at these two sites (Fig. 5). These values are also consistent with those observed by Meador et al. (2015) for IPL-BDGTs in the White Oak River Estuary, further suggesting a common source for BDGTs in these settings influenced by high inputs of terrestrial organic matter. By contrast,

255   $\delta^{13}C_{BDGTs}$ values in the sapropel layers of the Eastern Mediterranean Basin (GeoB15103) were up to 20‰ higher than $\delta^{13}C_{BDGTs}$ values in the sediments of the Rhone delta and Black Sea (Fig. 5).

A predominant methanotrophic origin for BDGTs is unlikely, as $\delta^{13}C_{BDGTs}$ values were generally higher than $\delta^{13}C_{CH4}$ (Fig. 5), which contrasts the relationship found in lipids from anaerobic methane-oxidizing archaea at seeps (Hinrichs et al., 1999; 2000). Pearson et al. (2010) reported fractionation effects (ε) between 7‰ and 36‰ between CO_2 and the produced biomass

260   in case of autotrophic pathways. In this study, $\Delta\delta^{13}C$ between CO_2 and BDGTs was calculated considering a fractionation of -10.7‰ between dissolved CO_2 and DIC in marine sediments (Mook et al., 1974; Fig. 5). In the Rhone delta and shallow Black Sea, $\Delta\delta^{13}C$ ranged between 21‰ and 45‰ in agreement with an autotrophic metabolism consistent with the initial suggestions by Meador et al. (2015). Alternatively, it cannot be excluded that the low $\delta^{13}C_{BDGTs}$ may be due to consumption of organic substrates that are more depleted in ^{13}C than bulk TOC. In addition, some methanogenic processes, based on CO_2 fixation

265   (hydrogenotrophic methanogenesis) or incorporation of methylated compounds (methylotrophic methanogenesis), induce large carbon isotopic fractionation during lipid biosynthesis (Londry et al., 2008; Summons et al., 1998) and could also explain the relatively low $\delta^{13}C_{BDGTs}$ values (i.e. < -20‰). On the contrary, in the sapropels and in the deeper horizon of the Black Sea, $\Delta\delta^{13}C_{CO2-BDGT}$ ranged between 9‰ and 12‰ (Fig. 5). This suggests an alternative carbon metabolism and/or phylogenetic group of BDGT producers. In particular, the heterotrophic incorporation of organic compounds usually induces a small isotopic

270   fractionation between the substrates and the membrane lipids (Pearson, 2010). Some methanogens can use acetate as a carbon source and a small isotopic fractionation has been observed in this case (Londry et al., 2008; Summons et al., 1998). This could hold true for the deep sample from the Black Sea. However, the relatively high concentrations of BDGTs and PDGTs in the Mediterranean sapropel samples (Suppl. Table 2) combined with low rates of methanogenesis, as indicated by the low CH_4 concentrations (Suppl. Table 1), strongly suggest that methanogens cannot account for the BDGT pool in this setting. It is

275   therefore likely that other archaea with non-methanogenic metabolisms are the sources of BDGTs in the Mediterranean sapropels.

Multivariate analysis of the marine sediment sample set (n = 48; Fig. 4) distinguished three BDGT and PDGT distribution patterns. The eastern Mediterranean Basin samples clustered with the other basin site samples of the dataset (Marmara Sea, Cap de Creus and Ligurian-Provençal Basin; Fig. 4). The Black Sea samples formed a second cluster and the Rhone delta samples formed the last cluster in the PCA. The first two clusters were characterized by a predominance of 1G-BDGTs (and 1G-PDGTs; Suppl. Table 2) but the Black Sea differed from the other basin sites due to higher proportions of CL-BDGTs than in the rest of the sample set as well as the absence of PDGTs. Additional contribution of BDGTs produced within the anoxic Black Sea bottom waters (Schröder, 2015) could explain the higher proportion of CL-BDGTs at this site. On the contrary, the last cluster (formed by Rhone delta samples) showed a predominance of 2G-BDGTs and 2G-PDGTs (Fig. 4). Meador et al. (2015) similarly observed a higher relative abundance of 2G-BDGTs and 2G-PDGTs in the White Oak River Estuary, another river mouth highly influenced by terrestrial input. By contrast, only 1G bearing BDGTs were observed in the membrane of *M. luminyensis* (Becker et al., 2016). This contrasted distribution pattern argues for a distinct, estuarine-based, archaeal community producing BDGTs.

Overall, our data infer that BDGT (and PDGT) producers may comprise an autotrophic, potentially methanogenic community as well as a heterotrophic, likely not methanogenic community. A methanogenic origin of BDGTs (and PDGTs) is in agreement with their prominence in *M. luminyensis* (Becker et al., 2016), the only cultured representative of Methanomassiliicoccales, a novel order of methanogens (Dridi et al., 2012). However, heterotrophic (acetate) C incorporation was so far suggested for Methanomassiliicoccales (Borrel et al., 2014; Lang et al., 2015; Söllinger et al., 2016), which cannot explain the observed carbon isotopic composition of BDGTs in the Rhone delta and the Black Sea if we consider the $\delta^{13}C$ of acetate to be similar to $\delta^{13}C_{TOC}$. More studies on Methanomassiliicoccales carbon metabolism are needed to accurately relate the presence of BDGTs in the environment to this archaeal group. Furthermore, the similar distributions of BDGTs and 16S rRNA gene clones from Bathyarchaeota in estuarine sediments led Meador et al. (2015) to suggest that this group is a putative source of BDGTs. Bathyarchaeota are widespread in marine sediments, notably in the deep subsurface horizons (e.g. Lloyd et al., 2013). They are phylogenetically highly diverse (e.g. Lazar et al., 2015) and contain diverse metabolic groups (e.g. Lazar et al., 2016; Yu et al., 2018; Zhou et al., 2018) involving both autotrophic and heterotrophic lifestyles. Methanogenic capacities have also been identified for some members of this clade (Evans et al., 2015). The contrasted BDGT carbon isotopic composition observed in the different sites of the present study could thus be explained by these versatile metabolic capabilities. It is thus conceivable that the ubiquitous Bathyarchaeota, including methanogens, are an additional source for BDGTs (and PDGTs) in the environment.

4.2 BDGTs as a putative adaptive trait of subsurface archaea

Zhu et al. (2014) demonstrated the 1,2,3 butanetriol structure of the BDGT backbone via gas chromatography MS, following ether cleavage from its biphytanyl chains. In the present study, 2D-NMR analysis confirmed the presence of a butanetriol backbone and unequivocally determined its configuration in the tetraether molecule (Fig. 2). Additional methylations have been previously observed on the isoprenoid chains or as methoxylation on the glycerol in different lipid classes (e.g. Elling et al., 2017; Knappy et al., 2015). However, BDGTs (and PDGTs) stand out as unique archaeal membrane lipids that contain a non-glycerol moiety. This raises two fundamental questions: (i) how are these lipids biosynthesized? and (ii) why do microorganisms produce them?

For every domain of life, it is known that dihydroxyacetone phosphate (DHAP), an intermediate in glycolysis, serves as a precursor of the glycerol moiety in membrane lipid backbones (Koga and Morii, 2007). At the early stage of membrane lipid biosynthesis, DHAP is converted by stereospecific glycerol dehydrogenase enzymes into either a glycerol-3-phosphate (G-3-P) or a glycerol-1-phosphate (G-1-P) in Bacteria and Archaea, respectively. The existence of BDGTs (and PDGTs) imply that different precursors must be involved at the very first steps of lipid biosynthesis. Knappy et al. (2014) suggested, for example, the involvement of putative butanetriol or pentanetriol phosphate. However, in the genomes of Methanomassiliicoccales, only

one gene for 3-O-geranylgeranyl-sn-glyceryl-1-phosphate (GGGP) synthase was identified (Becker et al., 2016), but no second homologue that might encode a hypothetical enzyme catalyzing the formation of butanetriol- or pentanetriol-based intermediates. Alternatively, BDGTs and PDGTs could be regular GDGTs, which underwent additional methylation at the final stages of their biosynthesis. Welander et al. (2010) showed that an S-adenosylmethionine (SAM) enzyme catalyzing a radical reaction was responsible for the methylation of certain bacterial hopanoids at the C2 position. We found 13 genes annotated as belonging to the radical SAM superfamily in the permanent draft genome of *M. luminyensis* B10 (IMG/M website, IMG Submission ID 11458; Chen et al., 2019). Very recently, another SAM enzyme was proposed to be involved in the biosynthesis of calditol based lipids in the archaeal strain *Sulfolobus acidocaldarius* (Zeng et al., 2018). A similar mechanism could explain the structure of BDGTs and PDGTs. The recent observation of such radical-mediated reactions on un-activated carbon atoms in both bacterial and archaeal strains (Zhou et al., 2016) implies that this may be a common mechanism to adapt their lipid envelope to the surrounding environment.

The ubiquitous presence of BDGTs and PDGTs in the environment and their active biosynthesis by certain organisms, notably *M. luminyensis* (Becker et al., 2016), signify that they have likely offered an evolutionary advantage to their producers. Two trends emerged from the concentration and distribution of BDGTs and PDGTs in the Mediterranean and the Black Seas. First, the proportion of BDGTs and PDGTs relative to GDGT-0 ((sum-BDGTs)/(sum-GDGT-0), (sum-PDGTs)/(sum-GDGT-0)) remained stable or even increased with depth (Suppl. Table 2). Moreover, unlike GDGT-0, the IPL form of BDGTs and PDGTs dominates their distribution at every depth (Fig. 3). This suggests that IPL-BDGTs and IPL-PDGTs may be specifically produced by sedimentary archaea, as Meador et al. (2015) previously proposed, and/or that they are more resistant against extracellular hydrolytic enzymes. The highest constraint for life in subsurface sediments is the lack of energy, which selects for microorganisms that limit their energy requirement to the most essential functions (e.g. Bradley et al., 2019; Hoehler and Jørgensen, 2013). Hypothetically, the additional methyl or ethyl group could increase the stability of the cell membrane by sterically hindering access of extracellular enzymes responsible for the lysis of the glycosidic bond that links the mono- or disaccharide headgroups, thereby preserving the IPL form and decreasing the maintenance energy demand of these organisms for lipid repair.

5 Conclusion

The unique structure of BDGTs, here unambiguously elucidated by NMR experiments, further increases the diversity of membrane lipids observed in Archaea. BDGTs and PDGTs were detected in a large set of marine sediment samples from diverse geochemical, depth and age conditions, highlighting their widespread presence in marine sediments. Within the dataset, major differences are also observed in the BDGT and PDGT headgroup distribution patterns and $^{13/12}C$ content of BDGT-derived biphytanes relative to DIC. Thus, it seems likely that BDGT and PDGT biosynthesis may be present across different archaeal phyla relying on different carbon metabolisms. A common trait of the subseafloor sample set is the high contribution of BDGTs, especially in their intact polar form, to the total lipid pool. The specific 1,2,3 butanetriol structure of their backbone could then be interpreted as an adaptive trait of sedimentary archaea to energy limited environments.

Data availability

Data will be made available in PANGAEA under https://doi.org/10.1594/PANGAEA.###.

Sample availability

Samples are stored at MARUM – Center for Marine Environmental Sciences, University of Bremen, Germany. Sample aliquots may be requested from Prof. Dr. Kai-Uwe Hinrichs.

Appendices

Supplementary Table 1: Sample general properties, organic matter and geochemical parameters.

Supplementary Table 2: Absolute concentration, relative abundance and distribution indices of GDGTs, BDGTs and PDGTs.

Supplementary Table 3: Carbon isotopic composition ($\delta^{13}C$) of the biphytanes derived from IPL-GDGT-0 and IPL-BDGT-0 together with the carbon isotopic composition of the total organic carbon (TOC), dissolved inorganic carbon (DIC) and methane.

Supplementary Figure 1: 1D ^1H spectrum and expansions of BDGT-0 in $CDCl_3$.

Supplementary Figure 2: ^1H-^{13}C HSQC two-dimensional spectra of BDGT-0.

Supplementary Figure 3: ^1H-^{13}C HMBC two-dimensional spectra of BDGT-0.

Author contribution

S.C., K.-U.H., J.S.L. and V.B.H. designed the study; S.C., T.B.M., K.W.B. and J.S. performed laboratory work and lipid quantification; L.M. and Q.-Z.Z. performed the isotope analysis; M.P.C. performed the NMR-based structural elucidation; V.B.H. selected sites and led sample collection and curation; S.C. performed the statistical analysis, interpreted the results and wrote the paper with significant input from T.B.M. and K.U.H.; all co-authors commented on the manuscript.

Competing interests

The authors declare that they have no conflict of interest.

Acknowledgements

The authors acknowledge the participants and the crew members of the two DARCSEAS cruises: RV *Meteor* Cruise M84/1 and RV *Poseidon* Cruise POS450. Jenny Wendt and Jessica Arndt are thanked for their help in the laboratory and for providing the CH_4 and DIC carbon isotopic compositions. We also thank the associate editor Dr. Marcel van der Meer, Dr. Darci Rush and an anonymous reviewer for their constructive comments that helped improve this manuscript. This study was funded by the European Research Council under the European Union's Seventh Framework Program – "Ideas" Specific Program, ERC grant agreement #247153 (Advanced Grant DARCLIFE; P.I. K.-U.H), the Deutsche Forschungsgemeinschaft through the Gottfried-Wilhelm Leibniz Program (Award HI 616-14-1) and by the University of Bremen through its excellence program "M8 Post-Doc Initiative" awarded to S.C. T.B.M. was additionally supported by MEYS CZ grant LM2015075 Projects of Large Infrastructure for Research, Development and Innovations as well as the European Regional Development Fund-Project: research of key soil-water ecosystem interactions at the SoWa Research Infrastructure (No. CZ.02.1.01/0.0/0.0/16_013/0001782).

References

Becker, K.W., Elling, F.J., Yoshinaga, M.Y., Söllinger, A., Urich, T., Hinrichs, K.-U.: Unusual butane- and pentanetriol-based tetraether lipids in *Methanomassiliicoccus luminyensis*, a representative of the seventh order of methanogens, Appl. Environ. Microbiol. 82, 4505–4516, AEM.00772-16, https://doi.org/10.1128/AEM.00772-16, 2016.

Becker, K.W., Lipp, J.S., Versteegh, G.J.M., Wörmer, L., Hinrichs, K.-U.: Rapid and simultaneous analysis of three molecular sea surface temperature proxies and application to sediments from the Sea of Marmara, Org. Geochem. 85, 42–53, https://doi.org/10.1016/j.orggeochem.2015.04.008, 2015.

Biddle, J.F., Lipp, J.S., Lever, M.A., Lloyd, K.G., Sørensen, K.B., Anderson, R., Fredricks, H.F., Elvert, M., Kelly, T.J., Schrag, D.P., Sogin, M.L., Brenchley, J.E., Teske, A., House, C.H., Hinrichs, K.-U.: Heterotrophic Archaea dominate sedimentary subsurface ecosystems off Peru, Proc. Natl. Acad. Sci. 103, 3846–3851, https://doi.org/10.1073/pnas.0600035103, 2006.

Borrel, G., Parisot, N., Harris, H.M., Peyretaillade, E., Gaci, N., Tottey, W., Bardot, O., Raymann, K., Gribaldo, S., Peyret, P., O'Toole, P.W., Brugère, J.-F.: Comparative genomics highlights the unique biology of Methanomassiliicoccales, a Thermoplasmatales-related seventh order of methanogenic archaea that encodes pyrrolysine, BMC Genomics 15, 679, https://doi.org/10.1186/1471-2164-15-679, 2014.

Bradley, J.A., Amend, J.P., LaRowe, D.E.: Survival of the fewest: Microbial dormancy and maintenance in marine sediments through deep time, Geobiology 17, 43–59, https://doi.org/10.1111/gbi.12313, 2019.

Chen, I.-M.A., Chu, K., Palaniappan, K., Pillay, M., Ratner, A., Huang, J., Huntemann, M., Varghese, N., White, J.R., Seshadri, R., Smirnova, T., Kirton, E., Jungbluth, S.P., Woyke, T., Eloe-Fadrosh, E.A., Ivanova, N.N., Kyrpides, N.C.: IMG/M v.5.0: an integrated data management and comparative analysis system for microbial genomes and microbiomes, Nucleic Acids Res. 47, D666–D677, https://doi.org/10.1093/nar/gky901, 2019.

De Rosa, M., Gambacorta, A.: The Lipids of Archaebacteria, Prog. Lipid Res. 27, 153–175, https://doi.org/10.1016/0163-7827(88)90011-2, 1988.

Dridi, B., Fardeau, M.-L., Ollivier, B., Raoult, D., Drancourt, M.: Methanomassiliicoccus luminyensis gen. nov., sp. nov., a methanogenic archaeon isolated from human faeces, Int. J. Syst. Evol. Microbiol. 62, 1902–1907, https://doi.org/10.1099/ijs.0.033712-0, 2012.

Elling, F.J., Könneke, M., Lipp, J.S., Becker, K.W., Gagen, E.J., Hinrichs, K.-U.: Effects of growth phase on the membrane lipid composition of the thaumarchaeon *Nitrosopumilus maritimus* and their implications for archaeal lipid distributions in the marine environment, Geochim. Cosmochim. Acta. 141, 579-597, https://doi.org/10.1016/j.gca.2014.07.005, 2014.

Elling, F.J., Könneke, M., Nicol, G.W., Stieglmeier, M., Bayer, B., Spieck, E., Torre, J.R. de la, Becker, K.W., Thomm, M., Prosser, J.I., Herndl, G.J., Schleper, C., Hinrichs, K.-U.: Chemotaxonomic characterisation of the thaumarchaeal lipidome, Environ. Microbiol. 19, 2681–2700, https://doi.org/10.1111/1462-2920.13759, 2017.

Evans, P.N., Parks, D.H., Chadwick, G.L., Robbins, S.J., Orphan, V.J., Golding, S.D., Tyson, G.W.: Methane metabolism in the archaeal phylum Bathyarchaeota revealed by genome-centric metagenomics, Science 350, 434–438, https://doi.org/10.1126/science.aac7745, 2015.

Hayes, J.M.: Fractionation of Carbon and Hydrogen Isotopes in Biosynthetic Processes, Rev. Mineral. Geochem. 43, 225–277, https://doi.org/10.2138/gsrmg.43.1.225, 2001.

Heuer, V.B., Aiello, I.W., Elvert, M., Goldenstein, N.I., Goldhammer, T., Könneke, M., Liu, X., Pape, T., Schmidt, F., Wendt, J., Zhuang, G.: Report and preliminary results of R/V POSEIDON cruise POS450, DARCSEAS II – Deep subseafloor Archaea in the Western Mediterranean Sea: Carbon Cycle, Life Strategies, and Role in Sedimentary Ecosystems, Barcelona (Spain) – Malaga (Spain), April 2 – 13, 2013 (No. 305), Berichte, MARUM – Zentrum für Marine Umweltwissenschaften, Fachbereich Geowissenschaften, Universität Bremen, Bremen, 2014.

Hinrichs, K.-U., Hayes, J.M., Sylva, S.P., Brewer, P.G., DeLong, E.F.: Methane-consuming archaebacteria in marine sediments Nature 398, 802–805, https://doi.org/10.1038/19751, 1999.

Hinrichs, K.-U., Summons, R.E., Orphan, V., Sylva, S.P., Hayes, J.M.: Molecular and isotopic analysis of anaerobic methane-oxidizing communities in marine sediments, Org. Geochem. 31, 1685–1701, https://doi.org/10.1016/S0146-6380(00)00106-6, 2000.

Hoefs, M.J.L., Schouten, S., Leeuw, J.W.D., King, L.L., Wakeham, S.G., Damsté, J.S.S.: Ether Lipids of Planktonic Archaea in the Marine Water Column, Appl. Env. Microbiol. 63, 3090–3095, 1997.

Hoehler, T.M., Jørgensen, B.B.: Microbial life under extreme energy limitation, Nat. Rev. Microbiol. 11, 83–94, https://doi.org/10.1038/nrmicro2939, 2013.

Kates, M.: The phytanyl ether-linked polar lipids and isoprenoid neutral lipids of extremely halophilic bacteria, Prog. Chem. Fats Other Lipids 15, 301–342, https://doi.org/10.1016/0079-6832(77)90011-8, 1977.

Kellermann, M.Y., Wegener, G., Elvert, M., Yoshinaga, M.Y., Lin, Y.-S., Holler, T., Mollar, X.P., Knittel, K., Hinrichs, K.-U.: Autotrophy as a predominant mode of carbon fixation in anaerobic methane-oxidizing microbial communities, Proc. Natl. Acad. Sci. 109, 19321–19326, https://doi.org/10.1073/pnas.1208795109, 2012.

Knappy, C., Barillà, D., Chong, J., Hodgson, D., Morgan, H., Suleman, M., Tan, C., Yao, P., Keely, B.: Mono-, di- and trimethylated homologues of isoprenoid tetraether lipid cores in archaea and environmental samples: mass spectrometric identification and significance, J. Mass Spectrom. 50, 1420–1432, https://doi.org/10.1002/jms.3709, 2015.

Knappy, C.S., Yao, P., Pickering, M.D., Keely, B.J.: Identification of homoglycerol- and dihomoglycerol-containing isoprenoid tetraether lipid cores in aquatic sediments and a soil, Org. Geochem. 76, 146–156, https://doi.org/10.1016/j.orggeochem.2014.06.003, 2014.

Koga, Y., Morii, H.: Recent Advances in Structural Research on Ether Lipids from Archaea Including Comparative and Physiological Aspects, Biosci. Biotechnol. Biochem. 69, 2019–2034, https://doi.org/10.1271/bbb.69.2019, 2005.

Koga, Y., Morii, H.: Biosynthesis of Ether-Type Polar Lipids in Archaea and Evolutionary Considerations, Microbiol. Mol. Biol. Rev. 71, 97–120, https://doi.org/10.1128/MMBR.00033-06, 2007.

Koga, Y., Nishihara, M., Morii, H., Akagawa-Matsushita, M.: Ether polar lipids of methanogenic bacteria: structures, comparative aspects, and biosynthesis, Microbiol. Rev. 57, 164–182, 1993.

Lang, K., Schuldes, J., Klingl, A., Poehlein, A., Daniel, R., Brune, A.: New Mode of Energy Metabolism in the Seventh Order of Methanogens as Revealed by Comparative Genome Analysis of "*Candidatus Methanoplasma termitum*", Appl. Environ. Microbiol. 81, 1338–1352, https://doi.org/10.1128/AEM.03389-14, 2015.

Lazar, C.S., Baker, B.J., Seitz, K., Hyde, A.S., Dick, G.J., Hinrichs, K.-U., Teske, A.P.: Genomic evidence for distinct carbon substrate preferences and ecological niches of Bathyarchaeota in estuarine sediments, Environ. Microbiol. 18, 1200–1211, https://doi.org/10.1111/1462-2920.13142, 2016.

Lazar, C.S., Biddle, J.F., Meador, T.B., Blair, N., Hinrichs, K.-U., Teske, A.P.: Environmental controls on intragroup diversity of the uncultured benthic archaea of the miscellaneous Crenarchaeotal group lineage naturally enriched in anoxic sediments of the White Oak River estuary (North Carolina, USA), Environ. Microbiol. 17, 2228-2238, https://doi.org/10.1111/1462-2920.12659, 2015.

Liu, X.-L., Summons, R.E., Hinrichs, K.-U.: Extending the known range of glycerol ether lipids in the environment: structural assignments based on tandem mass spectral fragmentation patterns, Rapid Commun. Mass Spectrom. 26, 2295–2302, https://doi.org/10.1002/rcm.6355, 2012.

Lloyd, K.G., Schreiber, L., Petersen, D.G., Kjeldsen, K.U., Lever, M.A., Steen, A.D., Stepanauskas, R., Richter, M., Kleindienst, S., Lenk, S., Schramm, A., Jørgensen, B.B.: Predominant archaea in marine sediments degrade detrital proteins, Nature 496, 215–218, https://doi.org/10.1038/nature12033, 2013.

Lombard, J., López-García, P., Moreira, D.: The early evolution of lipid membranes and the three domains of life, Nat. Rev. Microbiol. 10, 507–515, https://doi.org/10.1038/nrmicro2815, 2012.

Londry, K.L., Dawson, K.G., Grover, H.D., Summons, R.E., Bradley, A.S.: Stable carbon isotope fractionation between substrates and products of *Methanosarcina barkeri*, Org. Geochem. 39, 608–621, https://doi.org/10.1016/j.orggeochem.2008.03.002, 2008.

Meador, T.B., Bowles, M., Lazar, C.S., Zhu, C., Teske, A., Hinrichs, K.-U: The archaeal lipidome in estuarine sediment dominated by members of the Miscellaneous Crenarchaeotal Group: Archaeal lipid distributions in the WOR estuary, Environ. Microbiol. 17, 2441–2458, https://doi.org/10.1111/1462-2920.12716., 2015.

Meador, T.B., Gagen, E.J., Loscar, M.E., Goldhammer, T., Yoshinaga, M.Y., Wendt, J., Thomm, M., Hinrichs, K.-U.: *Thermococcus kodakarensis* modulates its polar membrane lipids and elemental composition according to growth stage and phosphate availability, Front. Microbiol. 5, https://doi.org/10.3389/fmicb.2014.00010, 2014.

480   Mook, W.G., Bommerson, J.C., Staverman, W.H.: Carbon isotope fractionation between dissolved bicarbonate and gaseous carbon dioxide, Earth Planet. Sc. Lett. 22, 169–176, https://doi.org/10.1016/0012-821X(74)90078-8, 1974.

Pancost, R.D., Bouloubassi, I., Aloisi, G., Sinninghe Damsté, J.S., Scientific Party, the M.S.: Three series of non-isoprenoidal dialkyl glycerol diethers in cold-seep carbonate crusts, Org. Geochem. 32, 695–707, https://doi.org/10.1016/S0146-6380(01)00015-8, 2001.

485   Paściak, M., Holst, O., Lindner, B., Mordarska, H., Gamian, A.: Novel Bacterial Polar Lipids Containing Ether-linked Alkyl Chains, the Structures and Biological Properties of the Four Major Glycolipids from *Propionibacterium propionicum* PCM 2431 (ATCC 14157 T), J. Biol. Chem. 278, 3948–3956, https://doi.org/10.1074/jbc.M206013200, 2003.

Pearson, A.: Pathways of Carbon Assimilation and Their Impact on Organic Matter Values δ13C, in: Handbook of Hydrocarbon and Lipid Microbiology, Springer, Berlin, Heidelberg, 143–156, https://doi.org/10.1007/978-3-540-77587-4_9, 490   2010.

Pearson, A., McNichol, A.P., Benitez-Nelson, B.C., Hayes, J.M., Eglinton, T.I.: Origins of lipid biomarkers in Santa Monica Basin surface sediment: A case study using compound-specific Δ^{14}C analysis, Geochim. Cosmochim. Acta 65, 3123–3137, 2001.

Pitcher, A., Hopmans, E.C., Schouten, S., Sinninghe Damsté, J.S.: Separation of core and intact polar archaeal tetraether lipids 495   using silica columns: Insights into living and fossil biomass contributions. Organic Geochemistry 40, 12–19. https://doi.org/10.1016/j.orggeochem.2008.09.008, 2009.

Reeburgh, W.S.: Oceanic Methane Biogeochemistry. Chem. Rev. 107, 486–513. https://doi.org/10.1021/cr050362v, 2007.

Rütters, H., Sass, H., Cypionka, H., Rullkötter, J.: Monoalkylether phospholipids in the sulfate-reducing bacteria *Desulfosarcina variabilis* and *Desulforhabdus amnigenus,* Arch. Microbiol. 176, 435–442, 500   https://doi.org/10.1007/s002030100343, 2001.

Schmidt, F., Koch, B.P., Goldhammer, T., Elvert, M., Witt, M., Lin, Y.-S., Wendt, J., Zabel, M., Heuer, V.B., Hinrichs, K.-U.: Unraveling signatures of biogeochemical processes and the depositional setting in the molecular composition of pore water DOM across different marine environments, Geochim. Cosmochim. Acta 207, 57–80, https://doi.org/10.1016/j.gca.2017.03.005, 2017.

505   Schouten, S., Hopmans, E.C., Pancost, R.D., Damsté, J.S.S.: Widespread occurrence of structurally diverse tetraether membrane lipids: Evidence for the ubiquitous presence of low-temperature relatives of hyperthermophiles, Proc. Natl. Acad. Sci. 97, 14421–14426, https://doi.org/10.1073/pnas.97.26.14421, 2000.

Schouten, S., Hopmans, E.C., Sinninghe Damsté, J.S.: The organic geochemistry of glycerol dialkyl glycerol tetraether lipids: A review, Org. Geochem. 54, 19–61, https://doi.org/10.1016/j.orggeochem.2012.09.006, 2013.

510   Schubotz, F., Lipp, J.S., Elvert, M., Hinrichs, K.-U.: Stable carbon isotopic compositions of intact polar lipids reveal complex carbon flow patterns among hydrocarbon degrading microbial communities at the Chapopote asphalt volcano, Geochim. Cosmochim. Acta 75, 4399–4415, https://doi.org/10.1016/j.gca.2011.05.018, 2011.

Schröder, J.M., Intact polar lipids in marine sediments: improving analytical protocols and assessing planktonic and benthic sources. PhD thesis, Universität Bremen, Bremen, Germany, 2015.

515   Sinninghe Damsté, J.S., Schouten, S., Hopmans, E.C., Duin, A.C.T. van, Geenevasen, J.A.J.: Crenarchaeol the characteristic core glycerol dibiphytanyl glycerol tetraether membrane lipid of cosmopolitan pelagic crenarchaeota, J. Lipid Res. 43, 1641–1651, https://doi.org/10.1194/jlr.M200148-JLR200, 2002.

Söllinger, A., Schwab, C., Weinmaier, T., Loy, A., Tveit, A.T., Schleper, C., Urich, T.: Phylogenetic and genomic analysis of Methanomassiliicoccales in wetlands and animal intestinal tracts reveals clade-specific habitat preferences, FEMS Microbiol.

520   Ecol. 92, fiv149, https://doi.org/10.1093/femsec/fiv149, 2016.

Sturt, H.F., Summons, R.E., Smith, K., Elvert, M., Hinrichs, K.-U.: Intact polar membrane lipids in prokaryotes and sediments deciphered by high-performance liquid chromatography/electrospray ionization multistage mass spectrometry—new biomarkers for biogeochemistry and microbial ecology, Rapid Commun. Mass Spectrom. 18, 617–628, https://doi.org/10.1002/rcm.1378, 2004.

525   Summons, R.E., Franzmann, P.D., Nichols, P.D.: Carbon isotopic fractionation associated with methylotrophic methanogenesis, Org. Geochem. 28, 465–475, https://doi.org/10.1016/S0146-6380(98)00011-4, 1998.

Vinçon-Laugier, A., Grossi, V., Pacton, M., Escarguel, G., Cravo-Laureau, C.: The alkyl glycerol ether lipid composition of heterotrophic sulfate reducing bacteria strongly depends on growth substrate, Org. Geochem. 98, 141–154, https://doi.org/10.1016/j.orggeochem.2016.05.015, 2016.

530   Weijers, J.W.H., Schouten, S., Hopmans, E.C., Geenevasen, J.A.J., David, O.R.P., Coleman, J.M., Pancost, R.D., Sinninghe Damsté, J.S.: Membrane lipids of mesophilic anaerobic bacteria thriving in peats have typical archaeal traits, Environ. Microbiol. 8, 648–657, https://doi.org/10.1111/j.1462-2920.2005.00941.x, 2006.

Welander, P.V., Coleman, M.L., Sessions, A.L., Summons, R.E., Newman, D.K.: Identification of a methylase required for 2-methylhopanoid production and implications for the interpretation of sedimentary hopanes, Proc. Natl. Acad. Sci. 107, 8537–

535   8542, https://doi.org/10.1073/pnas.0912949107, 2010.

Wessel, P., Smith, W.H.F., Scharroo, R., Luis, J., Wobbe, F.: Generic Mapping Tools: Improved Version Released, Eos 94, 409–410, https://doi.org/10.1002/2013EO450001, 2013.

Woese, C.R., Kandler, O., Wheelis, M.L.: Towards a Natural System of Organisms: Proposal for the Domains Archaea, Bacteria, and Eucarya, Proc. Natl. Acad. Sci. U. S. A. 87, 4576–4579, 1990.

540   Yu, T., Wu, W., Liang, W., Lever, M.A., Hinrichs, K.-U., Wang, F.: Growth of sedimentary Bathyarchaeota on lignin as an energy source, Proc. Natl. Acad. Sci. 115, 6022–6027, https://doi.org/10.1073/pnas.1718854115, 2018.

Zabel, M.: RV METEOR, Cruise Report M84/L1, Biogeochemistry and methane hydrates of the Black Sea; Oceanography of the Mediterranean; Shelf sedimentation and cold water carbonates. DFG Senatskommission für Ozeanographie c/o MARUM – Zentrum für Marine Umweltwissenschaften, Bremen, 2011.

545   Zeng, Z., Liu, X.-L., Wei, J.H., Summons, R.E., Welander, P.V.: Calditol-linked membrane lipids are required for acid tolerance in *Sulfolobus acidocaldarius*, Proc. Natl. Acad. Sci. 115, 12932–12937, https://doi.org/10.1073/pnas.1814048115, 2018.

Zhou, S., Alkhalaf, L.M., de los Santos, E.L., Challis, G.L.: Mechanistic insights into class B radical-S-adenosylmethionine methylases: ubiquitous tailoring enzymes in natural product biosynthesis, Curr. Opin. Chem. Biol. 35, 73–79,

550   https://doi.org/10.1016/j.cbpa.2016.08.021, 2016.

Zhou, Z., Pan, J., Wang, F., Gu, J.-D., Li, M.: Bathyarchaeota: globally distributed metabolic generalists in anoxic environments, FEMS Microbiol. Rev. 42, 639–655, https://doi.org/10.1093/femsre/fuy023, 2018.

Zhu, C., Lipp, J.S., Wörmer, L., Becker, K.W., Schröder, J., Hinrichs, K.-U.: Comprehensive glycerol ether lipid fingerprints through a novel reversed phase liquid chromatography–mass spectrometry protocol, Org. Geochem. 65, 53–62,

555   https://doi.org/10.1016/j.orggeochem.2013.09.012, 2013.

Zhu, C., Meador, T.B., Dummann, W., Hinrichs, K.-U.: Identification of unusual butanetriol dialkyl glycerol tetraether and pentanetriol dialkyl glycerol tetraether lipids in marine sediments, Rapid Commun. Mass Spectrom. 28, 332–338, https://doi.org/10.1002/rcm.6792, 2014.

 Table

Table 1: ^{13}C- and ^{1}H-NMR chemical shifts of BDGT-0 as well as key correlations from ^{1}H-^{13}C HSQC and HMBC spectra. Carbon numbers correspond to the carbon atoms in Fig. 2. Overlapped peaks are given as ranges (i.e. 1.17-1.21 ppm).

	δ ^{13}C (ppm)			δ ^{1}H (ppm)	Key correlations observed in the ^{1}H-^{13}C HSQC and HMBC spectra
Carbon number	CH$_3$	CH$_2$	CH		
A1		70.10		3.45	Strong degenerate methylene signal in ^{1}H-^{13}C HSQC; HMBC correlations to A2, A3 and C3 (across ether linkage).
A1'		68.78		3.56	Strong degenerate methylene signal in ^{1}H-^{13}C HSQC; HMBC correlations to A2' and A3' and C2' (across ether linkage).
B1		68.56		3.52 ; 3.64	See B2.
B1'		67.40		3.39 ; 3.58 (*dt, J* = 7.0, 8.8 Hz)	See B2' for correlations. Non-degenerate methylene pair.
A2		36.66		1.33 ; 1.59	^{1}H-^{13}C HMBC correlations to A1.
A2'		37.03		1.37 ; 1.58	Signals overlapped in ^{1}H-^{13}C HSQC but resolution afforded by ^{1}H-^{13}C HMBC correlations to A1', B1 and B1'.
B2		37.03		1.36 ; 1.60	
B2'		37.03		1.32 ; 1.57	
A3			29.71	1.51	Signals overlapped in ^{1}H-^{13}C HSQC, single positive (methine) signal observed, but A3, A3' resolved by HMBC. B3, B3' correlations too weak to distinguish due to multiplicity of B1, B1' correlations.
A3'			29.54	1.51	
B3, B3'			29.60	1.51	
A4, A4', B4, B4' A6, A6', B6, B6' A8, A8', B8, B8' A10, A10', B10, B10' A12, A12', B12, B12' A14, A14', B14, B14'		37.35		1.02-1.11; 1.21-1.27	
A5, A5', B5, B5' A9, A9', B9, B9' A13, A13', B13, B13'			24.36, 24.45	1.17-1.21; 1.27-1.30	
A7, A7', B7, B7' A11, A11', B11, B11' A15, A15', B15, B15'			32.75, 32.92	1.31-1.34	
A16, A16', B16, B16'		34.30		1.06 ; 1.22	
A17, A17', B17, B17'	19.70			0.85 - 0.87	Resolved from methyl group signals of A/B 18/18', 19/19' and 20/20' in ^{1}H-^{13}C HSQC. Two sets of doublets resolved in 1D but not assignable to A or B from 2D spectra.
A18, A18', B18, B18' A19, A19', B19, B19' A20, A20', B20, B20'	19.85			0.83 (app. D, *J* = 7.7 Hz)	Large apparent doublet arising from the 12 methyl groups.
Glycerol moiety					
C1		63.03		3.58 ; 3.68	^{1}H-^{13}C HSQC, methylene signal (negative), non-degenerate proton signals. Clear TOCSY correlations from 3.68 ppm

					(resolved) to 3.58, 3.51, 3.49 and 3.44 ppm. Weak ^{1}H-^{13}C HMBC correlation to C2, correlation to C3 also visible.
C2			78.31	3.49	
C3		71.07		3.44 ; 3.51	
Butanetriol moiety					
C1'		61.91		3.67 (d, J = 5.0 Hz)	^{1}H-^{13}C HSQC; single degenerate methylene resonance. ^{1}H-^{13}C HMBC; correlations to C2' and C3'.
C2'			82.38	3.17 (*dt*, J = 4.9, 5,3 Hz)	^{1}H-^{13}C HSQC; methine resonance, C-O chemical shift. ^{1}H-^{13}C HMBC; correlations weak due to multiplicity, but could observe correlation to A1' through ether linkage.
C3'			76.74	3.47	^{1}H-^{13}C HSQC; methine resonance, C-O chemical shift. ^{1}H-^{13}C HMBC; correlations to C2' and B1' (through ether linkage).
C4'	16.62			1.18 (d, J = 6.7 Hz but overlapped in 1D)	^{1}H-^{13}C HSQC; Single methyl resonance. ^{1}H-^{13}C HMBC; correlations to C2' and C3'. Characteristic coupling to C3' proton observed in ^{1}H-^{1}H COSY spectrum as well as correlations to C2' and C1' protons in the TOCSY spectrum.
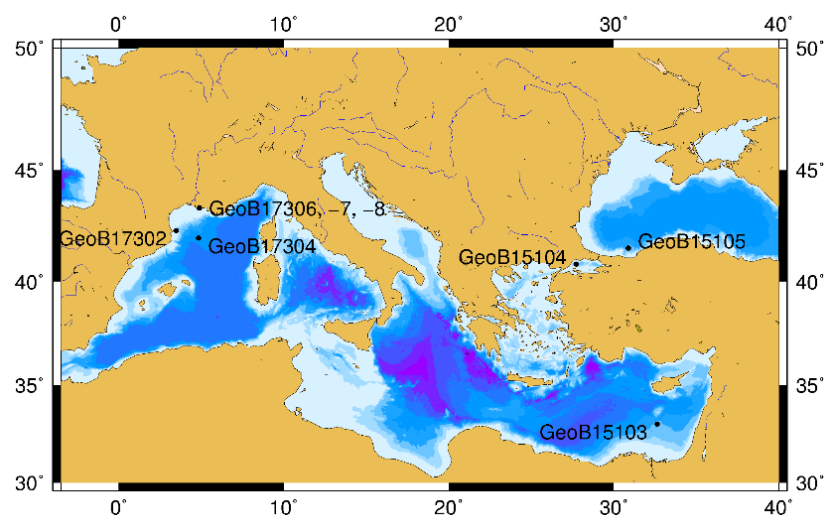
 Figures

Figure 1: Sampling sites in the Black Sea and Mediterranean Sea. The map was generated with GMT software (Wessel et al., 2013).
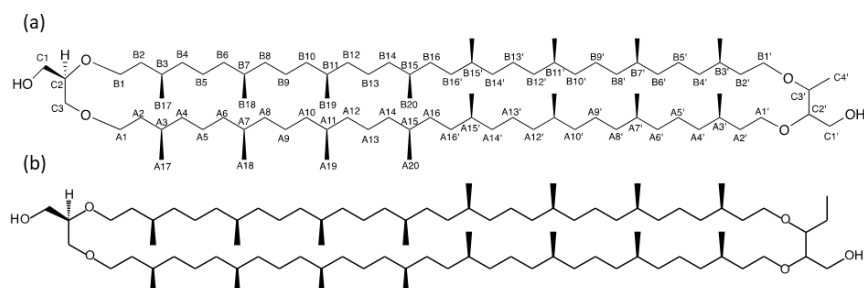
 Figure 2: Detailed structure of (a) BDGT-0 isolated from *M. luminyensis* and (b) hypothetical structure of PDGT-0 based on Zhu et al. (2014). Carbon numbers in (a) correspond to those given in Table 1, with C4' representing the additional carbon detected in BDGTs.
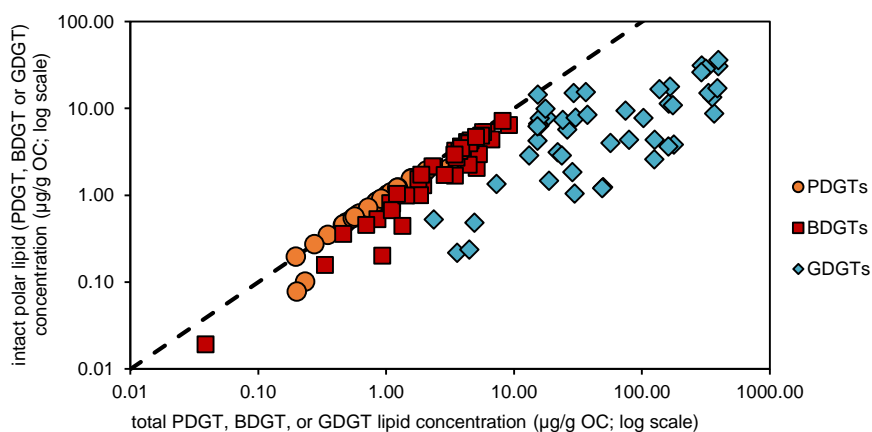
 Figure 3: Intact polar lipid concentration against total lipid concentration (log scales) for each archaeal lipid type discussed in this study (PDGTs in orange, BDGTs in red and GDGTs in blue). The dashed line represents the 1:1 line.
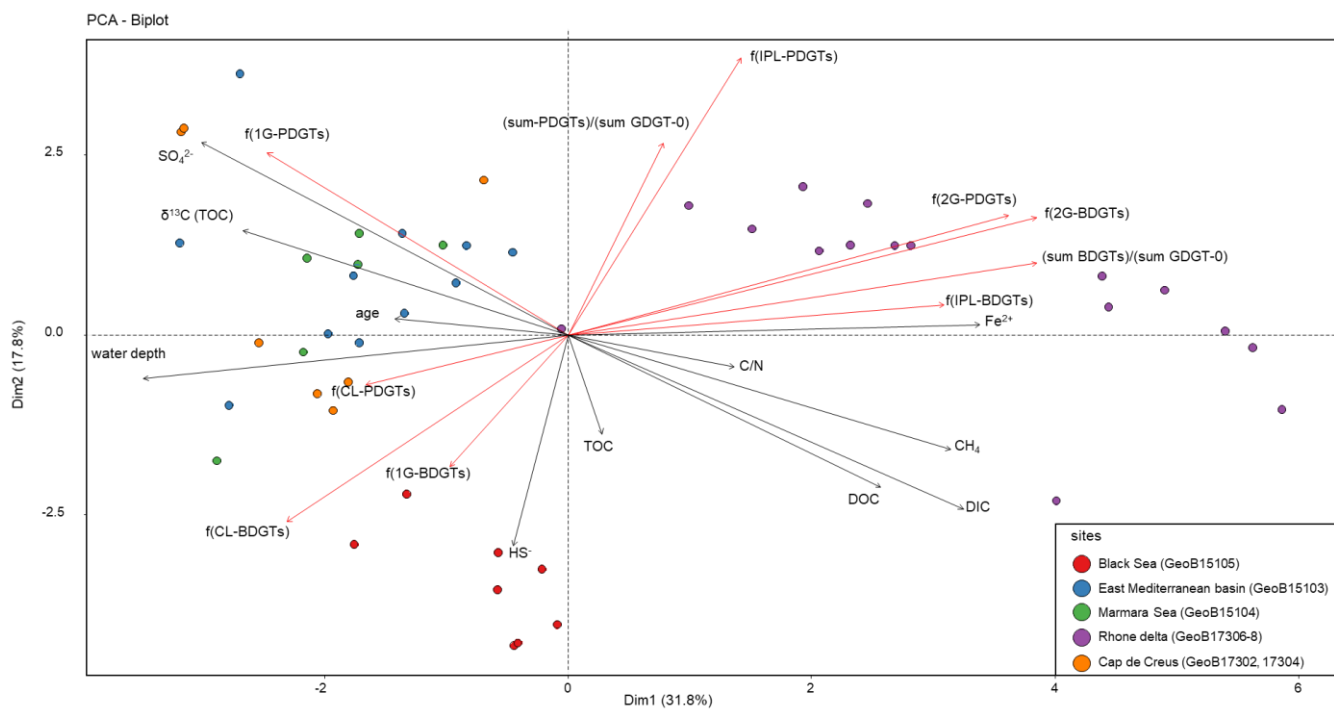
Figure 4: Principal Component Analysis (PCA) biplot showing relationships between major geochemical parameters (grey arrows), indices illustrating BDGT and PDGT distribution (red arrows), and 45 sediment samples (filled circles) from the Mediterranean and Black Seas where BDGTs and PDGTs were detected.
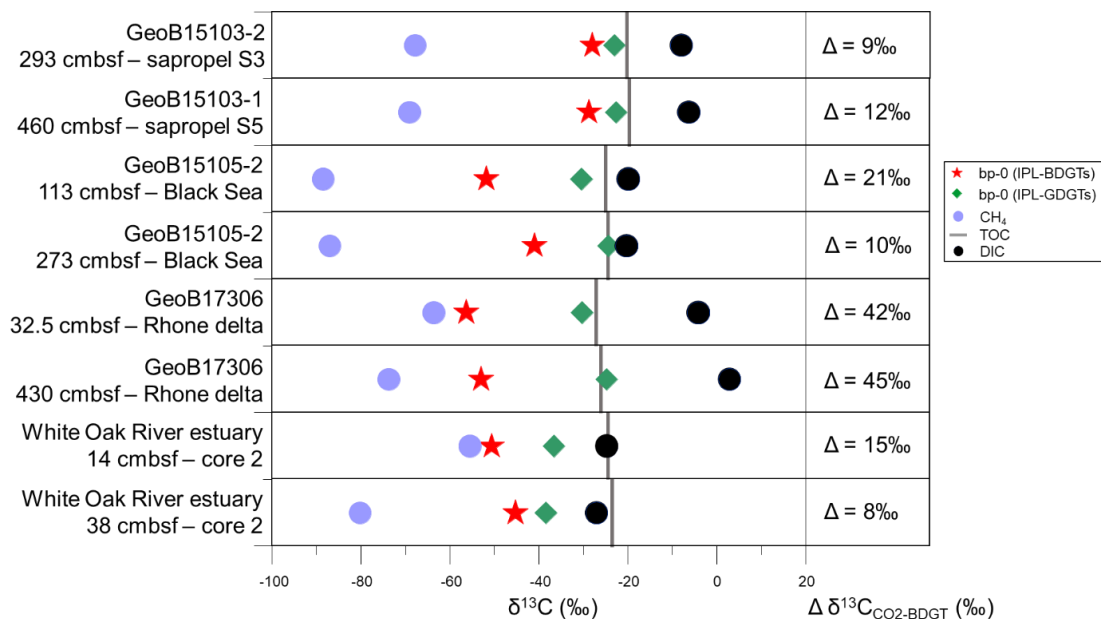
Figure 5: Stable carbon isotopic composition ($\delta^{13}C$) of bp-0 (IPL-BDGTs) (red stars), bp-0 (IPL-GDGTs) (green diamonds), CH_4 (light blue circles), DIC (black circles), TOC (grey bars) in six selected marine sediment samples from the Mediterranean Sea and Black Sea as well as from the White Oak River Estuary (Meador et al., 2015). Lipid samples were measured in duplicate and are presented as averages; deviations between individual measurements were generally smaller than the symbol size. On the right panel, the difference (Δ) between $\delta^{13}C_{CO2}$ and $\delta^{13}C_{BDGT}$ is computed for each sample. $\delta^{13}C_{CO2}$ was derived from $\delta^{13}C_{DIC}$ based on an isotope fractionation of -10.7‰ between dissolved CO_2 and DIC, considering in situ temperatures to be below 10 °C, according to Mook et al. (1974).